NANO LETTERS

Tuning Nonlinear Mechanical Mode Coupling in GaAs Nanowires Using Cross-Section Morphology Control

A. P. Foster,*,[†] J. K. Maguire,[†] J. P. Bradley,[†] T. P. Lyons,[†] A. B. Krysa,[‡] A. M. Fox,[†] M. S. Skolnick,[†] and L. R. Wilson[†]

[†]Department of Physics and Astronomy, University of Sheffield, Sheffield S3 7RH, United Kingdom
[‡]Department of Electronics and Electrical Engineering, University of Sheffield, Sheffield S1 3JD, United Kingdom

S *Supporting Information*

ABSTRACT: We investigate the nonlinear mechanical properties of GaAs nanowires with anisotropic cross-section. Fundamental and second order flexural modes are studied using laser interferometry with good agreement found between experiment and theory describing the nonlinear response under mechanical excitation. In particular, we demonstrate that the sign of the nonlinear coupling between orthogonal modes is dependent on the cross-section aspect ratio. The findings are of interest for applications such as amplitude to frequency conversion and vectorial force sensing.

KEYWORDS: *Semiconductor nanowire, morphology control, mechanical mode coupling, nonlinearity, elongated cross-section*
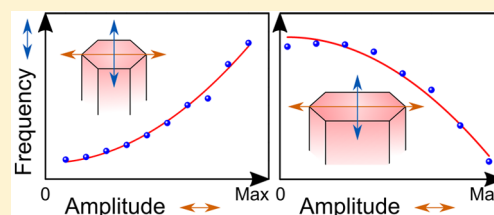
The mechanical properties of semiconductor nanowires have proven increasingly useful for a number of applications. These range from ultrasensitive detection of mass[1] and force[2,3] to coupling of the optical and mechanical degrees of freedom in heterostructure nanowires for use as hybrid quantum systems.[4,5] Applications such as these can naturally leverage the high mechanical quality factors expected for grown nanowires with atomically sharp facets and atomically abrupt clamping at the nanowire-substrate interface, particularly when compared to their etched counterparts that may suffer from surface[6] and clamping[7,8] induced losses. Furthermore, relatively high nanowire resonance frequencies result in decoupling of the motion from common sources of noise while improving force sensitivity.[9]

Nonlinear behavior is commonly encountered when investigating the dynamical properties of resonators such as nanowires[10,11] and cantilevers.[12,13] Nonlinearities are responsible for a wealth of interesting phenomena, including mechanical frequency mixing,[14] signal amplification,[15] and noise squeezing.[16] Nonlinear coupling between nanowire modes provides a means to determine the amplitude of one mode via a frequency measurement performed on a second mode, potentially enabling quantum nondemolition measurements of the mode occupancy.[17]

Recently, we demonstrated linearly polarized photon emission from an InGaAs quantum dot embedded in a GaAs nanowire through control of the nanowire cross-section aspect ratio.[18] Here, we show that tuning the aspect ratio can also be used to control the linear and nonlinear mechanical properties of GaAs nanowires. In particular, by determining the nanowire cross-section aspect ratio at the growth stage, we are able to control the sign of the nonlinear coupling between the fundamental flexural modes, and between the fundamental and second order flexural modes. We also show that,

independent of the aspect ratio, the initial dependence of the frequency of one mode on the squared amplitude of a coupled mode evolves into a linear relationship for larger motional amplitudes, which may be of particular interest for amplitude to frequency conversion applications.

The GaAs nanowires discussed here were produced using a bottom-up growth technique. Fabrication began with the deposition of 30 nm of SiO_2 on a (111)B GaAs substrate by plasma enhanced chemical vapor deposition. The SiO_2 growth mask was subsequently patterned into squares of 135 μm side length to moderate the nanowire growth rate.[19,20] Electron beam lithography and reactive ion etching were then used to pattern a single row of 20 apertures into each SiO_2 square. The apertures had a pitch of 4 μm and were either circular with diameter of ~120 nm or elongated with minor axis length of ~120 nm and varying major axis lengths. This allowed the cross-section of the resulting nanowires to be controlled. GaAs nanowires were grown from the apertures at 750 °C by metal organic vapor phase epitaxy using trimethylgallium (TMGa) and arsine (AsH_3) as precursors and hydrogen as a carrier gas. The reactor pressure and total gas flow were kept at 150 Torr and 18 standard liters per minute, respectively. The supply rates of TMGa and AsH_3 to the growth chamber were 5.2×10^{-5} and 6.3×10^{-4} mol/min, respectively. An AsH_3 overpressure was maintained during cooling of the sample to prevent degradation of the nanowires. Note that we have shown previously that there are three equivalent directions in which the elongation of the nanowire cross-section remains true to the elongation of the growth mask aperture due to the

symmetry of the hexagonal cross-section.[18] Here, we arbitrarily choose to align the major axis parallel to the major flat of the GaAs wafer.

Figure 1a shows a scanning electron microscope (SEM) image of a representative line of nanowires that have a diameter of ∼130 nm and height of ∼14.5 μm. The substrate has been
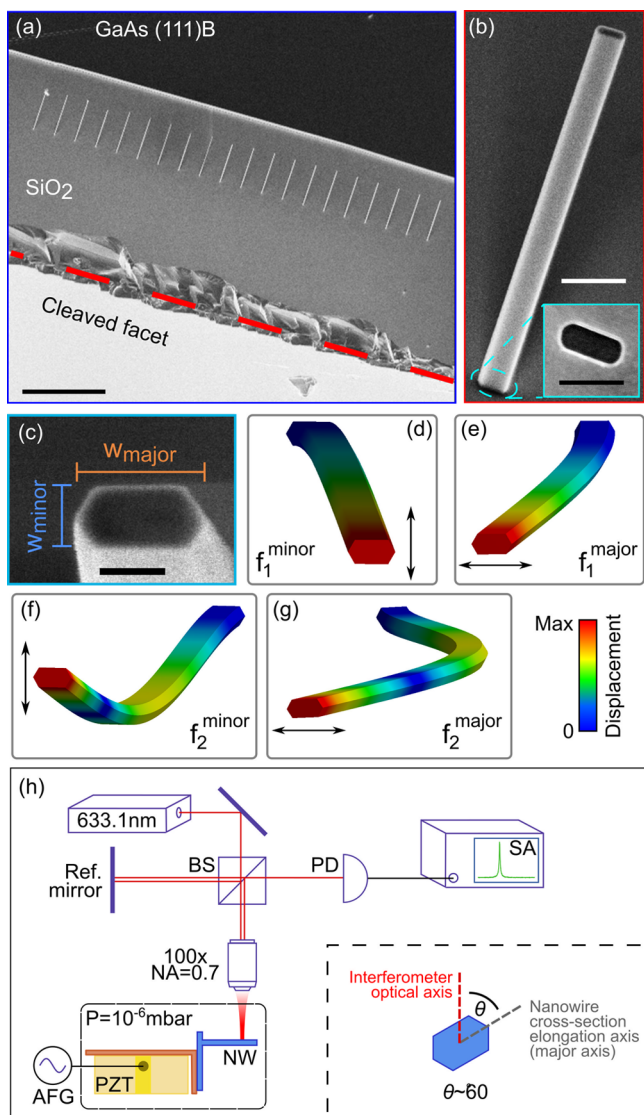

Figure 1. Scanning electron microscope (SEM) image of a line of vertical nanowires, with the (111)B GaAs substrate cleaved parallel to the line at a distance of ∼30 μm (shown by the dashed red line). Scale bar 20 μm. (b) Angled SEM image of a nanowire from a different array with an elongated cross-section. Scale bar 400 nm. (Inset) Top down SEM image of the aperture formed in the SiO$_2$ mask prior to nanowire growth. Scale bar 200 nm. (c) Shallow angle SEM image of a nanowire with cross-section aspect ratio of 2.25:1. Scale bar 100 nm. (d−g) Finite element simulations showing the orthogonal fundamental flexural mode shapes of the nanowire in (c) with lower frequency (d) f_1^{minor} and higher frequency (e) f_1^{major}, and the orthogonal second order modes shapes with frequency (f) f_2^{minor} and (g) f_2^{major}. (h) Simplified measurement schematic for the Michelson interferometer. (Inset) End view schematic of a nanowire, showing the orientation of the cross-section elongation axis relative to the interferometer optical axis. AFG, arbitrary function generator; BS, beam splitter; NW, nanowire; PD, photodetector; PZT, piezo transducer; ref. mirror, reference arm mirror; SA, spectrum analyzer.

cleaved parallel to the line of nanowires to facilitate optical detection of the mechanical motion, as explained later. Figure 1b shows an angled SEM image from a different array of a single nanowire with an elongated cross-section with the inset showing the aperture in the SiO$_2$ mask from which the nanowire was grown. Figure 1c shows a shallow angle SEM image of a nanowire with a cross-section aspect ratio (AR) equal to 2.25. We define the AR as the maximum width (w_{major}) along the major axis (the elongation direction) divided by the width along the minor axis (w_{minor}). Note that this means the AR is independent of the nanowire length. For the case of a nanowire with a regular hexagonal cross-section the orthogonal widths lead to an AR of $2/\sqrt{3}$ = 1.155. Figure 1d−g shows the fundamental and second order flexural mechanical mode shapes for a nanowire with an elongated cross-section determined from finite element method (FEM) simulations. For each flexural mode order i (=1, 2, ...) there exist two non-degenerate orthogonal modes due to the cross-section anisotropy. The FEM simulations show that the higher frequency mode vibrates in the plane formed by the nanowire growth axis and the cross-section elongation axis (the major axis). We refer to this mode as the major mode (with frequency f_i^{major}), and the orthogonal mode as the minor mode (f_i^{minor}). By choosing the elongation axis we are able to deterministically control the precise direction of motion of the orthogonal modes, unlike in the case of conventional nanowires with a small degree of random asymmetry in the cross-section.[2,10]

Nanowire motion was detected using a Michelson interferometer. The sensing laser was a wavelength stabilized diode operating at 633.1 nm. The sample was mounted on a right angled bracket attached to a piezo transducer (PZT) within a vacuum chamber. The nanowire growth axis was aligned perpendicular to the interferometer optical axis (Figure 1h). The sample was rotated about the nanowire growth axis such that the nanowire major axis was at ∼60° relative to the optical axis. This ensured that the orthogonal vibrational modes could be detected simultaneously. Prior to mounting, the sample was cleaved parallel to the rows of nanowires at a distance of ∼30 μm (see Figure 1a). This allowed a high NA objective (NA = 0.7, 100× magnification) to be used to focus the laser on a single nanowire without the substrate blocking a significant fraction of the incident and reflected laser fields. The photons reflected from the nanowire were interfered with photons returning from the Michelson reference arm on a variable gain photodiode, which was used in conjunction with a spectrum analyzer to determine the frequency response of the nanowire motion.

Measurements were undertaken at room temperature and a pressure of ∼10^{-6} mbar. The interferometer laser power was set at ∼2 μW to minimize heating of the sample.[2] We first consider three nanowires with AR = 1.17 (length × w_{major} × w_{minor} = 14.44 μm × 156 nm × 133 nm), AR = 1.72 (14.3 μm × 196 nm × 114 nm) and AR = 1.98 (12.88 μm × 244 nm × 123 nm). Figure 2a shows the fundamental thermomechanical mode spectra for these nanowires. The modes have room temperature quality factors (Q factors) of 2000−3000. The attribution of the modes was enabled by FEM simulations (as in Figure 1d−g) and confirmed by rotating the sample relative to the interferometer optical axis and determining when the major mode could no longer be measured, as in this case the nanowire major mode vibrates perpendicularly to the optical axis and thus cannot be resolved. Figure 2b shows the slight lifting of the degeneracy of the fundamental modes of the nanowire with AR
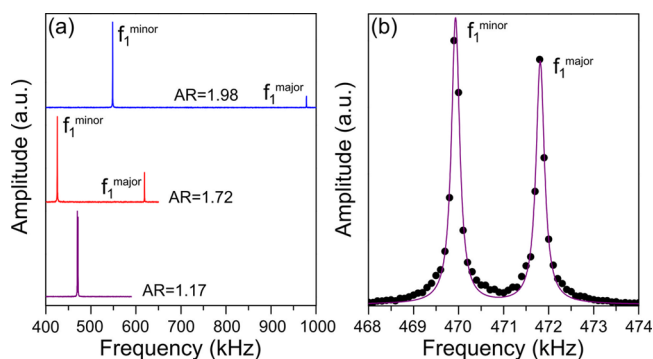
Figure 2. (a) Fundamental thermomechanical mode spectra for three nanowires with aspect ratio (AR) of 1.17, 1.72, and 1.98. The modes f_1^{major} and f_1^{minor} are orthogonal (see text). The spectra are scaled such that the maximum amplitude is the same in each case. The actual amplitude of thermomechanical motion is dependent on the spring constant associated with each mode, and the measured amplitude also depends on the detection angle. Spectra are offset in y for clarity. (b) Narrower bandwidth fundamental mode spectrum for the nanowire with an AR of 1.17, which has a nominally regular hexagonal cross-section. The mode splitting arises from the slight cross-section asymmetry of the nanowire. The experimental data (circles) is fitted with a double Lorentzian function (line).

= 1.17 in greater detail. The small frequency difference is commonly observed[4,10,11,21,22] and arises due to the seemingly unavoidable asymmetry inherent to nanowires with nominally regular hexagonal cross-section.

The average resonance frequencies for three sets of nanowires with average AR of 1.16, 1.64, and 2.00 and similar w_{minor} (115−135 nm) are summarized in Table 1. Resonance

Table 1. Average Resonance Frequencies for the First Four Flexural Modes for Nanowires with Three Different Average Cross-Section ARs[a]

AR	f_1^{minor} (kHz)	f_1^{major} (kHz)	f_2^{minor} (kHz)	f_2^{major} (kHz)
1.16 ± 0.07	461 ± 7	468 ± 10	2880 ± 40	2910 ± 40
1.64 ± 0.06	442 ± 15	651 ± 17	2770 ± 100	4080 ± 100
2.00 ± 0.07	542 ± 11	986 ± 15	3400 ± 70	6180 ± 100

[a]Averages are taken over 6, 8, and 8 nanowires for an AR of 1.16, 1.64, and 2.00, respectively. Errors are equal to one standard deviation in the nanowire dimensions for the AR and in the average measured frequencies otherwise.

frequencies of the order of 440−540 kHz are measured for f_1^{minor}, while the average value of $f_1^{major} - f_1^{minor}$ increases from ∼9 kHz for AR = 1.16 to ∼210 kHz (∼440 kHz) for AR = 1.64 (2.00). The increase in mode splitting is predominantly due to the nanowire dimension w_{major} increasing with the AR, as w_{minor}

is approximately constant across the arrays. Good agreement was found between the measured frequencies and those obtained from FEM simulations (within ∼1%, see Supporting Information), using a value of 130 GPa for the Young's modulus of GaAs. This is reasonably consistent with the bulk value of 141 GPa for GaAs in the [111] direction along which the nanowire growth axis lies.[23] The difference between the two values could potentially be due to rotational twin formation within the nanowires.[24] The absence of a diameter dependence of the Young's modulus suggests the difference is not the result of surface effects.[25]

Table 2 summarizes the measured frequency ratios for orthogonal modes of the same flexural order (f_1^{major}/f_1^{minor} and f_2^{major}/f_2^{minor}) and copolarized modes of differing order (f_2^{minor}/f_1^{minor} and f_2^{major}/f_1^{major}) for the same nanowires considered in Table 1. Regarding the former, Euler−Bernoulli beam theory predicts that $f_i^j \propto \sqrt{I_j}$ where I_j is the second moment of area pertaining to a mode vibrating in the direction j (= major or minor) and is independent of the mode number i. The orthogonal mode ratios are therefore given by $f_i^{major}/f_i^{minor} = \sqrt{I_{major}/I_{minor}}$. In the case of a beam with a rectangular cross-section, this value equals the ratio w_{major}/w_{minor} with the frequency of the major (minor) mode being linearly dependent on $w_{major(minor)}$. Here, we have used the exact expression for the second moment of area for each hexagonal cross-section nanowire with the calculated frequency ratios shown in the fourth column of Table 2 (see also Supporting Information Section S3). We see that the theory agrees very well with the measured values given in columns 2 and 3 of the same table. With regard to the copolarized mode ratios, we see that these are consistent with the value of 6.267 also obtained from Euler−Bernoulli beam theory. Note that calculations show that for a nanowire with an AR of 5.5, $f_1^{minor} + f_1^{major} \sim f_2^{minor}$, while for AR = 6.5, $f_1^{major} \sim f_2^{minor}$, two situations which are likely to lead to interesting mode coupling effects via internal resonances.[26,27]

It is well-known that a driven oscillator is liable to deviate from a linear response for sufficiently large response amplitude, resulting in the observation of nonlinear dynamics. With this in mind, we next investigate the behavior of each mode under swept mechanical excitation provided by the PZT attached to the sample. Figure 3 shows swept excitation measurements performed separately on the first and second flexural modes of two different nanowires with AR = 1.17 and AR = 1.98. For the smallest sweep amplitudes, the frequency f_{max} at which the maximum amplitude response is observed is approximately that of the linear resonance frequency. As the sweep amplitude is increased, the resonator begins to exhibit nonlinear behavior. This first manifests as a change in f_{max}, a phenomenon known

Table 2. Average Frequency Ratios for the First Four Flexural Modes for Nanowires with Three Different Average Cross-section ARs[a]

AR	f_1^{major}/f_1^{minor}	f_2^{major}/f_2^{minor}	E-B theory	f_2^{minor}/f_1^{minor}	f_2^{major}/f_1^{major}
1.16 ± 0.07	1.017 ± 0.015	1.005 ± 0.005	1.002 ± 0.080	6.272 ± 0.006	6.254 ± 0.031
1.64 ± 0.06	1.47 ± 0.04	1.47 ± 0.04	1.48 ± 0.03	6.269 ± 0.001	6.267 ± 0.001
2.00 ± 0.07	1.82 ± 0.02	1.82 ± 0.02	1.81 ± 0.07	6.267 ± 0.002	6.265 ± 0.006

[a]The fourth column gives the expected frequency ratios for the orthogonal modes calculated from Euler−Bernoulli (E-B) theory, which show good agreement with the experimentally determined ratios in columns two and three. The values in the final two columns agree with the value of 6.267 also calculated from E-B theory. Errors are equal to one standard deviation in the nanowire dimensions for AR and E-B theory and in the average measured frequency for the frequency ratios.
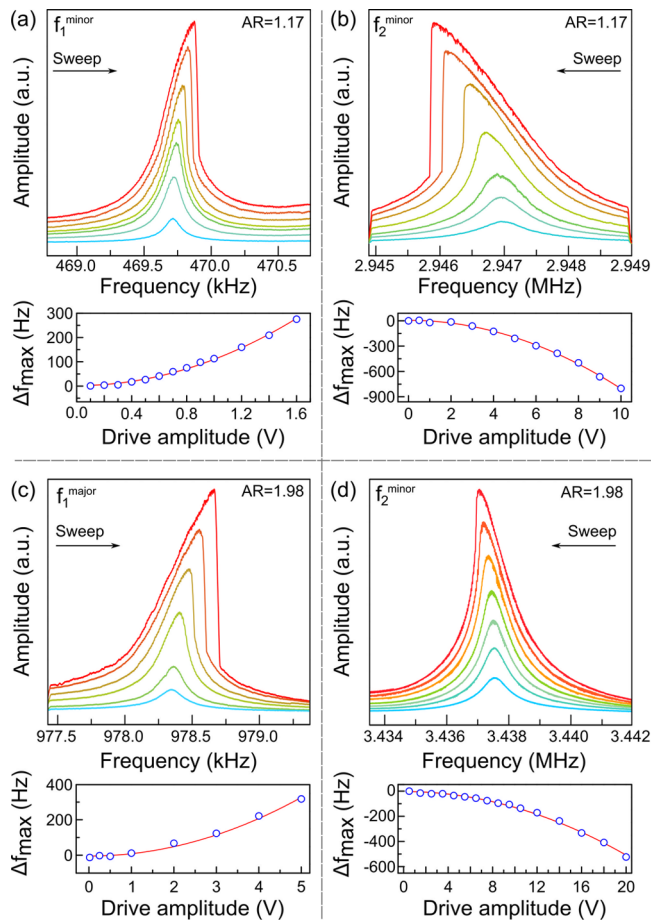
Figure 3. (Upper panels) Nanowire response amplitude under swept excitation for representative (a,c) fundamental and (b,d) second order flexural modes of nanowires with an AR of (a,b) 1.17 and (c,d) 1.98. The drive amplitude increases from the bottom trace to the top trace in each case. Note that for (a,c) the interferometer detection laser was focused near the clamping point of the nanowire to prevent compression of the optical signal at large amplitudes. (Lower panels) Change in the frequency at maximum response amplitude f_{max} versus drive amplitude. The experimental data points (circles) are fit with a quadratic function (lines) in each case.

as spring stiffening or spring softening depending on whether f_{max} increases or decreases. Eventually, the system enters a bistable regime, characterized by a step change in amplitude at a critical sweep frequency. The frequency at which this occurs is dependent on the drive amplitude and the initial conditions (in this case governed by the sweep direction). Note that the different sweep directions used for the two cases plotted in Figure 3 were chosen simply to show maximum frequency pulling. For the relatively large amplitudes required to observe nonlinear behavior here, the interferometer detection scheme itself becomes nonlinear with higher harmonics appearing for amplitudes greater than the interferometer fringe width ($\lambda/4$, $\lambda = 633.1$ nm). On the basis of the interferometer response, we estimate that the amplitude at the onset of nonlinear motion of the f_1 modes is of the order of 1 μm, while for the f_2 modes the amplitude is less than the fringe width (~160 nm). An upper limit on the amplitude of the f_i^{major} modes is given by the 4 μm separation of adjacent nanowires in the major direction (hence an amplitude of 8 μm).

For all values of the AR considered here the f_1^{minor} and f_1^{major} modes exhibit spring stiffening, consistent with reports in the

literature for nanowires with regular hexagonal cross-section.[10,11] In contrast, the f_2^{minor} and f_2^{major} modes exhibit spring softening with f_{max} reduced relative to the linear resonance frequency. The change in f_{max} as a function of drive amplitude is plotted in the lower panels of Figure 3, revealing a quadratic dependence in each case. The observation of either spring stiffening or spring softening for a particular mode was found to be independent of the AR within the limits of the ARs considered here.

We can understand the observed behavior by modeling the nanowire as a damped, driven harmonic oscillator with a nonlinear restoring force. By writing the mode as $u(x, t) = a(t)\xi(x)$ with mode shape $\xi(x)$, the dimensionless equation of motion for the time dependent amplitude $a(t)$ is the Duffing equation[12]

$$\ddot{a} + \mu\dot{a} + \omega^2 a + \gamma_1 \delta a^3 + \gamma_2 \delta(a\dot{a}^2 + a^2\ddot{a}) = F(\Omega, t) \quad (1)$$

Here μ is the linear damping coefficient, $\omega/2\pi$ is the linear resonance frequency, $\delta = (w/L)^2$ with w the nanowire width in the direction of motion of the mode and L the nanowire length, and F is a function of the time dependent driving force with frequency Ω. The cubic nonlinearity parametrized by the coefficient γ_1 arises due to the geometric nonlinearity and is responsible for the drive amplitude dependence of f_{max} for the fundamental flexural modes.[12] For this case, it can be shown[28] that f_{max} has a quadratic dependence on the amplitude of the driving force as seen experimentally in Figure 3. The fifth term in eq 1 is due to the inertial nonlinearity and has been shown to dominate the behavior of the second flexural mode in cantilevers, giving rise to spring softening.[12,26] This is in agreement with the spring softening behavior observed here for the f_2 modes. The magnitude of the experimentally observed cubic nonlinearity can be estimated from the expression $32\pi^2 f_{lin} (f_{max} - f_{lin})x^2/3$, where f_{lin} is the linear resonance frequency and x is the amplitude at f_{max}.[29] For the nanowires discussed here, estimates for the magnitude of the cubic nonlinearity of 10^{21} (ms)$^{-2}$ and 10^{25} (ms)$^{-2}$ are obtained for the f_1 and f_2 modes, respectively, using the expected nonlinear amplitudes discussed previously. In comparison, for f_1 modes ref 22 reports a value of 10^{21} (ms)$^{-2}$ for silicon nanowires and ref 11 reports a value of 10^{23} (ms)$^{-2}$ for GaAs nanowires (at low temperature hence higher Q factor). As demonstrated in ref 11, the geometric nonlinearity in GaAs nanowires is sufficiently large to allow for applications such as nonlinear mechanical mixing. Note that the nonlinear coefficient scales with δ[12] hence can be tuned via this parameter.

The geometric nonlinearity also results in coupling between the nanowire modes, whereby the frequency of one mode is dependent on the amplitude of other modes. For coupled major and minor modes $u(x, t) = a(t)\xi(x)$ and $v(x, t) = b(t)\xi(x)$ with linear mode shape $\xi(x)$, the dimensionless equations of motion derived from ref 30 are

$$\ddot{a} + \mu_{minor}\dot{a} + \omega_{minor}^2 a + \frac{D_{min}}{D_{maj}}\gamma_1\delta a^3 + \left[\frac{D_{min}}{D_{maj}}\gamma_1 - \rho_1\left(1 - \frac{D_{min}}{D_{maj}}\right)\right.$$

$$\left. + \rho_2 \frac{D_{maj}}{D_k}\left(1 - \frac{D_{min}}{D_{maj}}\right)^2\right]\delta ab^2 = F_{minor}(\Omega, t) \quad (2)$$

and

$$\ddot{b} + \mu_{\text{major}}\dot{b} + \omega_{\text{major}}^2 b + \gamma_1 \delta b^3 + \left[\gamma_1 + \rho_1 \left(1 - \frac{D_{\text{min}}}{D_{\text{maj}}} \right) \right.$$

$$\left. + \rho_2 \frac{D_{\text{maj}}}{D_k} \left(1 - \frac{D_{\text{min}}}{D_{\text{maj}}} \right)^2 \right] \delta b a^2 = F_{\text{major}}(\Omega, t)$$

$$(3)$$

including the geometric nonlinearity only (see Supporting Information). Here, $\omega_j/2\pi$ is the linear resonance frequency of mode j (= major or minor), μ_j is the damping coefficient, γ_1, ρ_1 and ρ_2 are mode coupling coefficients related to the mode shape, $\delta = (w_{\text{minor}}/L)^2$ and F_j is a time dependent function of the driving force with frequency Ω. D_j is the bending stiffness related to motion of mode j, while D_k is the torsional stiffness. The ratio $D_{\text{min}}/D_{\text{maj}}$ is proportional to $(w_{\text{minor}}/w_{\text{major}})^2$ (see Supporting Information). Equations 2 and 3 result in the frequency of mode $u(x,t)$ having a quadratic dependence on the amplitude $b(t)$ of mode $v(x,t)$.[10,31,32] In the case of a nanowire with an approximately regular hexagonal cross-section, $D_{\text{min}}/D_{\text{maj}} \sim 1$ and eqs 2 and 3 reduce to the system investigated in ref 10. The equations describe the mode coupling in the framework of Euler−Bernoulli beam theory, which therefore places a lower limit on the ratio of the nanowire length to width for which the theory is valid. This ratio is of the order of 10 (as shown experimentally for SiN cantilevers[33]) implying a lower limit on the length of ∼1−3 μm for the nanowires investigated here (which are longer than 10 μm in each case). The validity of eqs 2 and 3 also requires that the torsional frequencies be much higher than the flexural mode frequencies, a condition which is satisfied for lengths greater than ∼1−5 μm for the nanowires studied here with an AR of 1.17−2.75 (see Supporting Information). Crespo da Silva and Zaretzky have developed a theoretical model for the case where torsional modes are of comparable frequency to the flexural modes.[34,35]

We first experimentally demonstrate coupling of the fundamental flexural modes, f_1^{minor} and f_1^{major}. For nanowires with either AR = 1.17 or 1.72, driving either mode results in spring stiffening of the orthogonal mode. Figure 4a,b shows the frequency pulling due to spring stiffening observed in the case of driving mode f_1^{major} and detecting mode f_1^{minor} in each case. The frequency pulling is seen to have a quadratic dependence on the drive amplitude for small amplitudes. Upon increasing the AR further to 1.98, a change in sign of the coupling is observed resulting in spring softening of the coupled mode (Figure 4c). We confirmed that this remains the case for a nanowire with an even greater AR of 2.75 (dimensions of 12 μm × 347 nm × 126 nm).

The change in sign of the mode coupling can be understood by considering the terms in ab^2 in eq 2, which describes the behavior of the minor mode. The parameters γ_1, ρ_1, and ρ_2 have values for the fundamental modes of 40.44, −20.22, and −16.61, respectively (see Supporting Information). Consider the case where we drive mode f_1^{major} and measure the frequency of f_1^{minor}, as in Figure 4a−c. As the nanowire AR increases, the ratio $D_{\text{minor}}/D_{\text{major}}$ decreases from an initial value of unity (the case for a nanowire with a regular hexagonal cross-section). The sum of the first two terms in ab^2 is positive for all AR and increases linearly with increasing AR. The torsion-dependent third term is negative for all AR and becomes rapidly more negative with increasing AR due both to the quadratic dependence on $(1 - D_{\text{minor}}/D_{\text{major}})$ and the fact that D_{major}/D_k increases with increasing AR (see Supporting Information). The term in ab^2 therefore changes sign from positive to
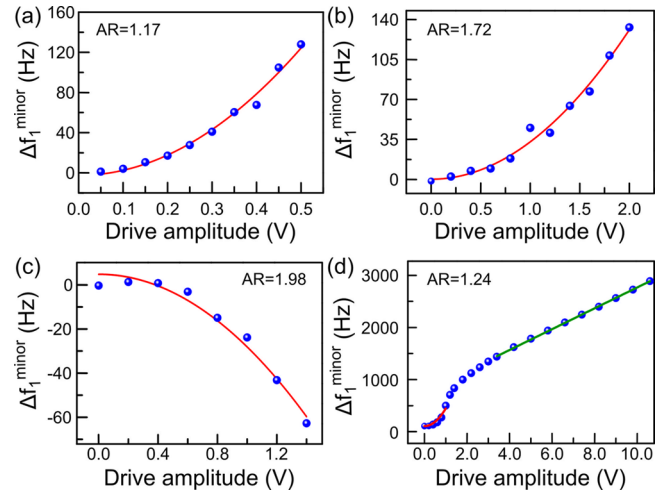

Figure 4. Spring stiffening observed for mode f_1^{minor} when driving mode f_1^{major} in the case of nanowires with an AR of (a) 1.17 and (b) 1.72. (c) Spring softening of mode f_1^{minor} when driving mode f_1^{major} for a nanowire with AR = 1.98. In (a−c), measured data points are given by circles and red lines are quadratic fits to the data. (d) Transition from quadratic to linear spring stiffening of mode f_1^{minor} when driving mode f_1^{major} for a nanowire with an AR of 1.24. The red line is a quadratic fit to the experimental data (blue circles) for small drive amplitudes and the green line is a linear fit to the data for large drive amplitudes.

negative with increasing AR. This leads to a transition from spring stiffening to spring softening with increasing AR and provides a new route to control the mode coupling in nano- and microcantilevers. Note that driving the f_1^{minor} mode has exactly the same effect on the f_1^{major} mode as in the reverse case discussed above. From our experimental results, it can be deduced that for a nanowire with an elongated hexagonal cross-section there exists for 1.72 < AR < 1.98 an AR for which the quadratic coupling between the fundamental modes disappears and for small driven amplitudes there should be no observable coupling to the orthogonal fundamental mode. Calculations show that the change in sign should occur for AR ∼ 2.05 (see Supporting Information). The slight discrepancy could arise from other potential sources of nonlinearity, such as imperfect surfaces (e.g., the effect of a native oxide) or crystal defects (for instance due to rotational twinning). The proximity of the experimental and theoretical values implies that such an effect is however a relatively small perturbation.

The data in Figure 4a−c can be characterized in terms of the resonance frequency shift of the undriven mode as a function of the squared amplitude of the driven mode. Given the uncertainty in the driven mode amplitude, this is estimated to lie in the range 10^{-5}−10^{-3} Hz nm^{-2} for the fundamental modes. Note that the AR for which zero mode coupling is observed is independent of the strength of the nonlinearity when the behavior is described by eqs 2 and 3. Note also that as the mode coupling strength is a function of the AR, the strongest coupling occurs either for the minimum AR of 1.155 or for AR larger than ∼2.75 (see Figure S4 in Supporting Information).

Figure 4d shows frequency pulling of mode f_1^{minor} due to driving mode f_1^{major} for a nanowire with AR = 1.24 with the data extended relative to that in Figure 4a−c to include much larger drive amplitudes. We see a distinct change in behavior of the mode coupling, with the quadratic frequency pulling observed

at low drive voltage developing into a linear frequency pulling regime. The same change was observed for nanowires with AR = 1.72 and AR = 1.98. Note that we confirmed that the PZT displacement responsible for the driving force increased linearly over the entire voltage range used in this measurement (see Supporting Information). When the Duffing oscillator as described by eq 1 is driven at the linear resonance frequency, the amplitude response as a function of the drive amplitude can initially be considered to be linear but then develops a cube root dependence as the oscillator becomes strongly nonlinear. The frequency of a second mode quadratically coupled to the driven mode as described by eq 2, might therefore be expected to show a drive amplitude dependence which would transition from V^2 to $V^{2/3}$ with increasing drive strength, which is in contrast to our observation here. Observation of a V^2 to $V^{2/3}$ transition has been reported in the case of clamped−clamped resonators[31] and was attributed in that case to entering the strong bending regime of motion.[36]

The origin of linear frequency pulling for large drive amplitude in the system discussed here is unclear, but could arise for a number of reasons. These include entering the strong bending regime for a nanowire (rather than the clamped−clamped beam case mentioned above), nonlinear damping, or additional sources of nonlinearity arising from imperfect surfaces, rotational twin defects and nonlinear elastic constants. The calculated maximum strain experienced by the nanowires is of the order of 0.25% (see Supporting Information), well below the breaking strain reported for GaAs nanowires[37] but potentially large enough to show nonlinear elastic behavior. Ultimately, the behavior we observe means that is it possible to envisage a system where correct choice of the nanowire cross-section AR reduces the quadratic coupling between modes to zero with the larger amplitude coupling then entirely of linear nature after an initial lower amplitude region exhibiting zero coupling.

Coupling between the first and second order flexural modes has also been observed. Figure 5a,b shows the frequency of modes f_1^{minor} and f_1^{major} as a function of the drive amplitude of either mode f_2^{minor} or f_2^{major} for a nanowire with AR = 1.17. When the driven and detected modes are copolarized, spring softening of the undriven mode is observed. Spring stiffening is seen for the undriven mode when the driven mode is orthogonally polarized. The form of the amplitude-frequency dependence is not clear when driving the second flexural modes and monitoring the fundamental modes due to the limited PZT response at MHz frequencies. We confirmed that in the reverse case a quadratic dependence is observed as for the case of driving and detecting fundamental modes only. This is shown in Figure 5c,d in which mode f_1^{major} is driven while the frequency of mode f_2^{minor} is measured for two nanowires with AR of 1.17 and 1.98, respectively. As in the case of the orthogonal fundamental modes discussed in Figure 4, a change in sign of the mode coupling is observed with increasing AR. In contrast, Figure 5e,f shows that when driving and measuring copolarized modes (in this case driving f_1^{minor} and measuring the frequency of f_2^{minor}) no change in sign is observed. This is as expected from eqs 2 and 3, because for copolarized modes $D_{minor} = D_{major}$, hence in this case there is no dependence of the sign of the mode coupling on the AR.

In conclusion, we have demonstrated control of nonlinear mechanical mode coupling in grown GaAs nanowires through control of the nanowire cross-section aspect ratio. Driving one of the fundamental flexural modes results in spring stiffening of
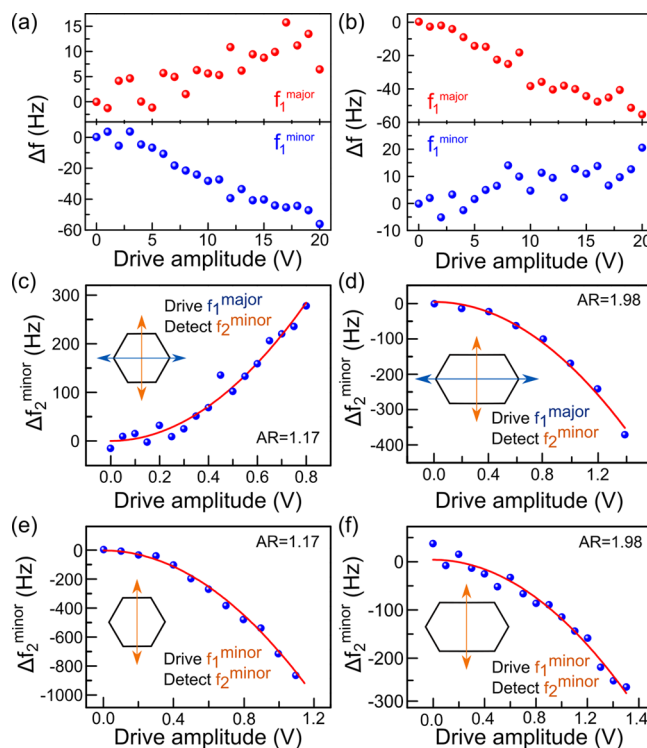

Figure 5. Frequency pulling observed for modes f_1^{minor} and f_1^{major} due to driving mode (a) f_2^{minor} and (b) f_2^{major} for a nanowire with an AR of 1.17. (c−f) Frequency pulling observed for mode f_2^{minor} due to driving mode (c,d) f_1^{major} and (e,f) f_1^{minor}. In (c,e) AR = 1.17 and in (d,f) AR = 1.98.

the orthogonal fundamental mode for nanowires with regular hexagonal cross-section. Upon increasing the cross-section aspect ratio to 2:1 the mode coupling presents as spring softening of the undriven coupled mode. We have also shown that driving a mode at resonance into the nonlinear regime leads to a linear dependence of the coupled mode frequency on the driven mode amplitude in contrast to the sublinear response predicted by the Duffing equation. Finally, we have investigated the behavior of the second flexural modes, which show frequency softening under swept excitation. The stiffening or softening response of a second order mode when a coupled fundamental mode is driven is also shown to depend on the nanowire cross-section aspect ratio. Our fundamental studies provide new information about mechanical mode coupling in nanowires that is relevant for applications such as amplitude to frequency conversion and vectorial force sensing. Future studies could focus on additional factors such as nanowire surface and growth quality or investigate the very large amplitude regime where material nonlinearities may become important.

■ ASSOCIATED CONTENT

Ⓢ Supporting Information

The Supporting Information is available free of charge on the ACS Publications website at DOI: 10.1021/acs.nano-lett.6b02994.

FEM calculation of mechanical modes of hexagonal cross-section nanowires and nanowire strain under large deformation, determination of relevant bending stiffness for each mode, derivation of coupled mode equations, linearity of PZT amplitude with drive voltage (PDF)

■ AUTHOR INFORMATION

Corresponding Author

*E-mail: andrew.foster@sheffield.ac.uk.

Notes

The authors declare no competing financial interest.

■ REFERENCES

(1) Feng, X. L.; He, R.; Yang, P.; Roukes, M. L. *Nano Lett.* **2007**, *7*, 1953−1959.

(2) Rossi, N.; Braakman, F. R.; Cadeddu, D.; Vasyukov, D.; Tütüncüoglu, G.; Fontcuberta i Morral, A.; Poggio, M. *Nat. Nanotechnol.* [Online early access]. DOI: 10.1038/nnano.2016.189. Published Online: Oct 17, 2016. http://www.nature.com/nnano/journal/vaop/ncurrent/full/nnano.2016.189.html (accessed Oct 31, 2016).

(3) Gloppe, A.; Verlot, P.; Dupont-Ferrier, E.; Kuhn, A. G.; Siria, A.; Poncharal, P.; Bachelier, G.; Vincent, P.; Arcizet, O. *Int. Conf. Opt. MEMS Nanophotonics* **2014**, *9*, 73−74.

(4) Montinaro, M.; Wüst, G.; Munsch, M.; Fontana, Y.; Russo-Averchi, E.; Heiss, M.; Fontcuberta i Morral, A.; Warburton, R. J.; Poggio, M. *Nano Lett.* **2014**, *14*, 4454−4460.

(5) Yeo, I.; de Assis, P.-L.; Gloppe, A.; Dupont-Ferrier, E.; Verlot, P.; Malik, N. S.; Dupuy, E.; Claudon, J.; Gérard, J.-M.; Auffèves, A.; Nogues, G.; Seidelin, S.; Poizat, J.; Arcizet, O.; Richard, M. *Nat. Nanotechnol.* **2013**, *9*, 106−110.

(6) Yang, J.; Ono, T.; Esashi, M. *Appl. Phys. Lett.* **2000**, *77*, 3860−3862.

(7) Ko, J. H.; Jeong, J.; Choi, J.; Cho, M. *Appl. Phys. Lett.* **2011**, *98*, 171909.

(8) Ekinci, K. L.; Roukes, M. L. *Rev. Sci. Instrum.* **2005**, *76*, 061101.

(9) Rast, S.; Wattinger, C.; Gysin, U.; Meyer, E. *Nanotechnology* **2000**, *11*, 169−172.

(10) Cadeddu, D.; Braakman, F. R.; Tütüncüoglu, G.; Matteini, F.; Rüffer, D.; Fontcuberta i Morral, A.; Poggio, M. *Nano Lett.* **2016**, *16*, 926−931.

(11) Braakman, F. R.; Cadeddu, D.; Tütüncüoglu, G.; Matteini, F.; Rüffer, D.; Fontcuberta i Morral, A.; Poggio, M. *Appl. Phys. Lett.* **2014**, *105*, 173111.

(12) Venstra, W. J.; Westra, H. J. R.; van der Zant, H. S. J. *Appl. Phys. Lett.* **2010**, *97*, 193107.

(13) Venstra, W. J.; Westra, H. J. R.; van der Zant, H. S. J. *Appl. Phys. Lett.* **2011**, *99*, 151904.

(14) Erbe, A.; Krommer, H.; Kraus, A.; Blick, R. H.; Corso, G.; Richter, K. *Appl. Phys. Lett.* **2000**, *77*, 3102−3104.

(15) Rugar, D.; Grutter, P. *Phys. Rev. Lett.* **1991**, *67*, 699−702.

(16) Almog, R.; Zaitsev, S.; Shtempluck, O.; Buks, E. *Phys. Rev. Lett.* **2007**, *98*, 078103.

(17) Santamore, D. H.; Doherty, A. C.; Cross, M. C. *Phys. Rev. B: Condens. Matter Mater. Phys.* **2004**, *70*, 144301.

(18) Foster, A. P.; Bradley, J. P.; Gardner, K.; Krysa, A. B.; Royall, B.; Skolnick, M. S.; Wilson, L. R. *Nano Lett.* **2015**, *15*, 1559−1563.

(19) Makhonin, M. N.; Foster, A. P.; Krysa, A. B.; Fry, P. W.; Davies, D. G.; Grange, T.; Walther, T.; Skolnick, M. S.; Wilson, L. R. *Nano Lett.* **2013**, *13*, 861−865.

(20) Kumakura, K.; Nakakoshi, K.; Kishida, M.; Motohisa, J.; Fukui, T.; Hasegawa, H. *J. Cryst. Growth* **1994**, *145*, 308−313.

(21) Hallstrom, W.; Lexholm, M.; Suyatin, D. B.; Hammarin, G.; Hessman, D.; Samuelson, L.; Montelius, L.; Kanje, M.; Prinz, C. N. *Nano Lett.* **2010**, *10*, 782−787.

(22) Nichol, J. M.; Hemesath, E. R.; Lauhon, L. J.; Budakian, R. *Appl. Phys. Lett.* **2009**, *95*, 123116.

(23) Brantley, W. A. *J. Appl. Phys.* **1973**, *44*, 534−535.

(24) Chen, Y.; Burgess, T.; An, X.; Mai, Y.-W.; Tan, H. H.; Zou, J.; Ringer, S. P.; Jagadish, C.; Liao, X. *Nano Lett.* **2016**, *16*, 1911−1916.

(25) Wang, Y. B.; Wang, L. F.; Joyce, H. J.; Gao, Q.; Liao, X. Z.; Mai, Y. W.; Tan, H. H.; Zou, J.; Ringer, S. P.; Gao, H. J.; Jagadish, C. *Adv. Mater.* **2011**, *23*, 1356−1360.

(26) Pai, P. F.; Nayfeh, A. H. *Int. J. Non. Linear. Mech.* **1990**, *25*, 455−474.

(27) Crespo da Silva, M. R. M.; Zaretzky, C. L. *Int. J. Non. Linear. Mech.* **1990**, *25*, 227−239.

(28) *The Duffing Equation: Nonlinear Oscillators and their Behaviour*; Kovacic, I.; Brennan, M. J., Eds.; Wiley: New York, 2011.

(29) *Nonlinear oscillations*; Nayfeh, A. H., Mook, D. T., Eds.; Wiley: New York, 1995.

(30) Crespo da Silva, M. R. M.; Glynn, C. C. *J. Struct. Mech* **1978**, *6*, 449−461.

(31) Westra, H. J. R.; Poot, M.; van der Zant, H. S. J.; Venstra, W. J. *Phys. Rev. Lett.* **2010**, *105*, 117205.

(32) Truitt, P. A.; Hertzberg, J. B.; Altunkaya, E.; Schwab, K. C. *J. Appl. Phys.* **2013**, *114*, 114307.

(33) Villanueva, L. G.; Karabalin, R. B.; Matheny, M. H.; Chi, D.; Sader, J. E.; Roukes, M. L. *Phys. Rev. B: Condens. Matter Mater. Phys.* **2013**, *87*, 024304.

(34) Zaretzky, C. L.; Crespo da Silva, M. R. M. *Nonlinear Dyn.* **1994**, *5*, 161−180.

(35) Zaretzky, C. L.; Crespo da Silva, M. R. M. *Nonlinear Dyn.* **1994**, *5*, 3−23.

(36) Sapmaz, S.; Blanter, Y. M.; Gurevich, L.; van der Zant, H. S. J. *Phys. Rev. B: Condens. Matter Mater. Phys.* **2003**, *67*, 235414.

(37) Bao, P.; Wang, Y.; Cui, X.; Gao, Q.; Yen, H. W.; Liu, H.; Kong Yeoh, W.; Liao, X.; Du, S.; Hoe Tan, H.; Jagadish, C.; Zou, J.; Ringer, S. P.; Zheng, R. *Appl. Phys. Lett.* **2014**, *104*, 021904.